

Scientists develop retina E-paper display with 25k pixels per inch, matching human vision

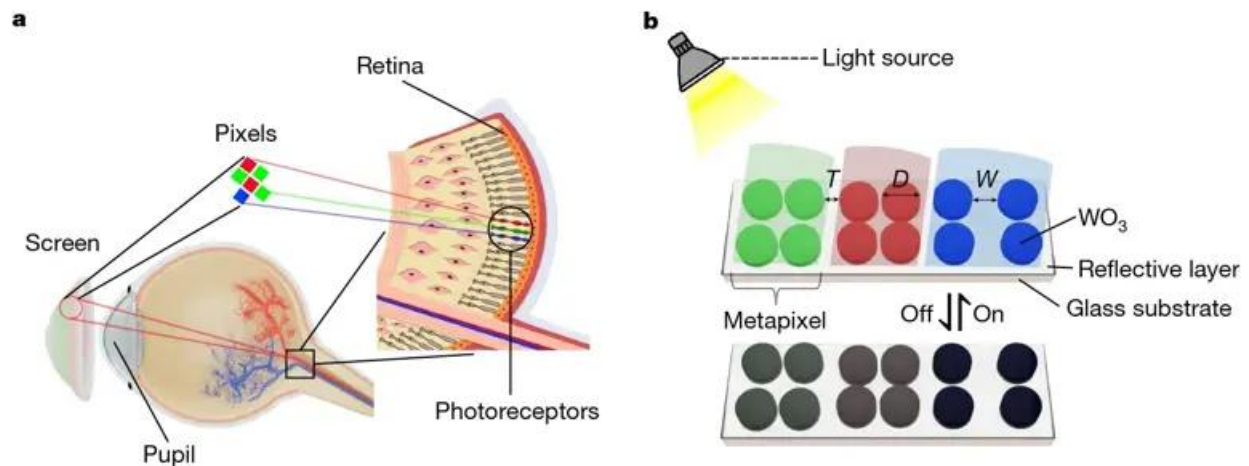


Scientists in Sweden have created a revolutionary new form of “electronic paper” that could change the way we interact with screens — from smartphones and laptops to next-generation virtual and augmented reality headsets.

In a paper, published in the journal *Nature*, scientists have created retina electronic paper, or retina E-paper, capable of showing realistic color pictures with pixels smaller than a single human photoreceptor.

Shrinking Pixels to Match Human Vision

When you hold a phone against your face or wear a VR headset, the screen resolution determines how real the image feels. The more tightly engineers squeeze pixels together to sharpen them, the faster they reach hard limits — colors merge, brightness diminishes, and it becomes costly to build. Emissive screens, which are the type used in most displays today, suffer from a difficulty when pixel dimensions drop to a micrometer or so.



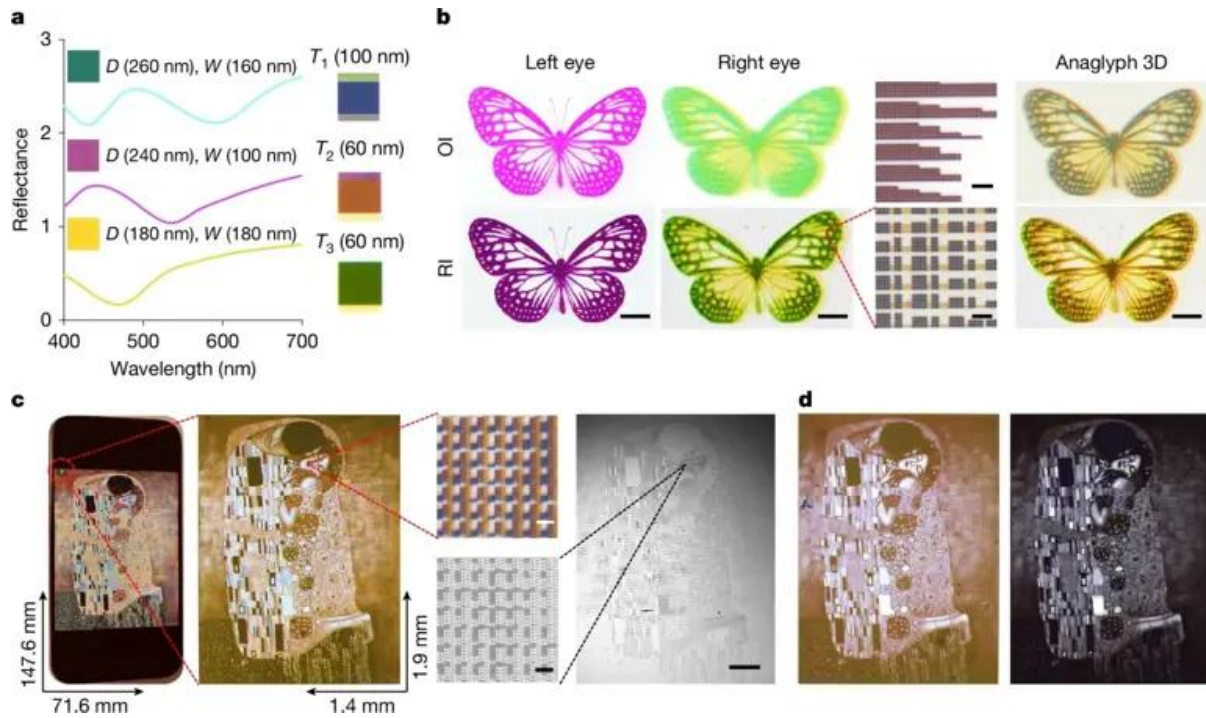
Conceptual illustration of an ultimate virtual reality display. The display is sized to approximate the human pupil and features an ultra-high pixel density serving as a conceptual benchmark inspired by the retina, supporting ultra-fine visual detail.

Reflective screens, on the other hand, bounce ambient light back off instead of radiating it. They provide better brightness and reduced power usage, but previously, they've lacked the clarity of high-end OLEDs. The Swedish scientists desired to reverse this situation and develop a screen so subtle it would rival the precise nature of the human eye.

Their objective was lofty: to produce over 23,000 pixels an inch, roughly what the retina can perceive viewing an image through a pore the size of an eyeball. What they achieved was staggering, with more than 25,000 pixels an inch — the most accurate display ever produced.

The Science Behind the Smallest Pixels

At their core are metapixels — nanoscale pixels composed of small tungsten trioxide (WO_3) disks placed on reflective metal surfaces. The disks are a few hundred nanometers in diameter, smaller than viruses in most instances. By tweaking the size and spacing of the disks, the researchers were able to cause each disk to reflect specific colors — red, green, and blue — which, when combined together, can produce the whole range of colors.



Characterization of retina E-paper display performance.

WO_3 is special since it's electrochromic: it changes its optical property when small ions, such as lithium, move in and out of its form. This switching between metallic and insulating modes alters the light-reflection property of the material. In effect, a very small electrical pulse can “turn on” or “turn off” a pixel, altering its color or brightness without the need for power.

That is incredible efficiency. The retina E-paper consumes nearly 1.7 milliwatts per square centimeter when playing video and drops down to roughly 0.5 milliwatts for still images. Even after the power is switched off, colors remain in place for tens of minutes — a “color memory” effect that keeps power consumption low.

Performance That Rivals Reality

While tiny, these metapixels are video-speed, shifting states as rapidly as 40 milliseconds — fast enough for smooth motion. Reflectance of bright state is roughly 80 percent, with a light-to-dark contrast ratio of roughly 50 percent. Color is deep and saturated even when pixels are minimized, ending the age-old problem in display design.



Andreas Dahlin, Professor, the Department of Chemistry and Chemical Engineering, Chalmers University of Technology, Sweden

To demonstrate the capabilities of the technology, the team copied Gustav Klimt's "The Kiss" onto a 1.4 by 1.9 millimeter area — about one four-thousandth the area of a smartphone screen — but with the same resolution.

They also printed a full-color picture of a butterfly and even a 3D illusion with distinct color channels for each eye, showing the system's ability to handle complex, dynamic images.

This means that each pixel is roughly equal to one photoreceptor in the eye,” says Andreas Dahlin, professor at [Chalmers University of Technology](#). “Humans cannot see anything beyond this resolution.”

Kunli Xiong, the paper’s lead author and assistant professor at Uppsala University, further added that the technology opens up new ways to engage with information and the world. “It could broaden creative horizons, facilitate remote collaboration, and even accelerate scientific inquiry,” he said.



Giovanni Volpe, Professor, the Department of Physics, University of Gothenburg, Sweden.

Toward the Next Generation of VR and AR

Because retina E-paper is reflective rather than emissive, it is able to display realistic images with reduced power consumption and eye fatigue. That makes it an ideal candidate for virtual and augmented reality systems, where light-weight and power-frugal displays are critical.

Researchers imagine small devices in which the screen is no bigger than an eye’s pupil but gives a broad field of view with human-level acuity. The low

energy requirement also suggests self-sustaining applications that might be combined with [solar cells](#), eliminating the need for constant charging.

But there are obstacles on the road ahead to commercial deployment. The gamut of color available with the current system is not as broad as with OLED displays, and the materials must survive millions of switching cycles. Large-scale implementations will require advanced thin-film transistor arrays to address each pixel independently — a significant engineering challenge.

However, the researchers believe that this technology is a breakthrough. “This is a significant development in the production of screens that can be made smaller while improving quality and reducing energy consumption,” professor at the [University of Gothenburg](#) Giovanni Volpe says.



Kunli Xiong, Associate senior lecturer/Assistant Professor, the Department of Materials Science and Engineering, Uppsala University, Sweden. (

Practical Implications of the Research

The arrival of retina E-paper could redefine display technology across sectors. To users, it will mean [VR headsets](#) and smart glasses that feel more natural and less power-hungry. To scientists and designers, it is an entirely new canvas on which to show information at resolutions previously not attainable.

In education and communications, it can make digital areas more realistic, allowing professionals and students to collaborate remotely as though they were in the same location.

By operating through ambient light and drawing small amounts of power, it can lead to greener, more durable devices — a step towards sustainable digital screens.

Research findings are available online in the journal [Nature](#).

Video-rate tunable color electronic paper with human resolution

- [Ade Satria Saloka Santosa, Yu-Wei Chang, Andreas B. Dahlin, Lars Österlund, Giovanni Volpe & Kunli Xiong](#)
- [Nature](#) Published: 22 October 2025

Abstract

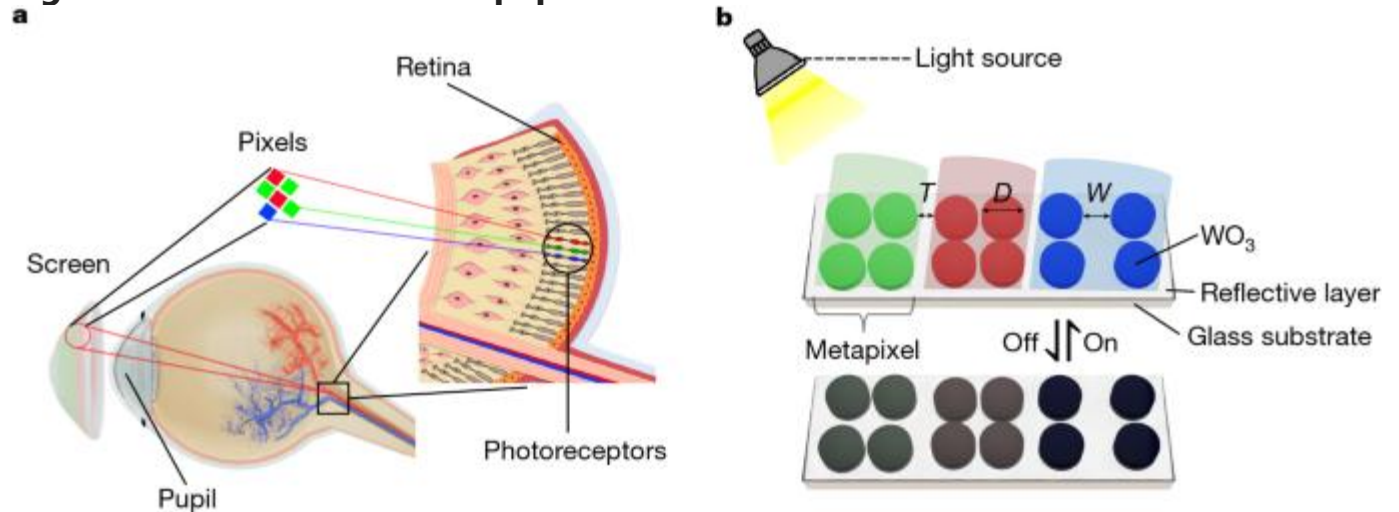
As demand for immersive experiences grows, displays with smaller sizes and higher resolutions are being viewed increasingly closer to the human eye¹. As the size of emitting pixels shrinks, the intensity and uniformity of their emission are degraded while colour cross-talk and fabrication complexity increase, making ultra-high-resolution imaging challenging^{2-3,4}. By contrast, electronic paper, which uses ambient light for visibility, can maintain high optical contrast regardless of pixel size, but cannot achieve high resolution^{5,6}. Here we demonstrate electronic paper with electrically tunable metapixels down to ~560 nm in size (>25,000 pixels per inch) consisting of

WO₃ nanodisks, which undergo a reversible insulator-to-metal transition on electrochemical reduction. This transition enables dynamic modulation of the refractive index and optical absorption, allowing precise control over reflectance and contrast at the nanoscale. By using this effect, the metapixels can achieve pixel densities approaching the visual resolution limit when the display size matches the pupil diameter, which we refer to as retina electronic paper. Our technology also demonstrates full-colour video capability (>25 Hz), high reflectance (~80%), strong optical contrast (~50%), low energy consumption (~0.5–1.7 mW cm⁻²) and support for anaglyph 3D display, highlighting its potential as a next-generation solution for immersive virtual reality systems.

Main

From cinema screens and televisions, to smartphones and virtual reality headsets, displays have progressively moved closer to the human eye, featuring smaller sizes and higher resolutions. As display technology advances, a fundamental question arises regarding the ultimate limits of display size and resolution. To provide an immersive and high-fidelity visual experience, the display is designed with a size comparable to the human pupil and an ultra-high pixel density. It establishes a conceptual benchmark inspired by the resolving limits of the retina (Fig. 1a) and defines a practical boundary for display technologies, which we term the retina display.

Fig. 1: Schematic of retina E-paper.



a, Conceptual illustration of an ultimate virtual reality display. The display is sized to approximate the human pupil and features an ultra-high pixel density serving as a conceptual benchmark inspired by the retina, supporting ultra-fine visual detail. **b**, Structural diagram of metapixels (subpixels). The metapixels consist of WO_3 nanodisks and a reflective layer on a glass substrate. By varying D and W of the nanodisks, the metapixels can selectively reflect RGB colours. Further tuning of T enables the generation of hybrid colours such as CMY. As WO_3 is electrochromic it can undergo reversible electrochemical reactions, yielding reflectance modulation of the WO_3 nanodisks, enabling an RGB video display.

Assuming an effective display aperture of 8 mm, corresponding to the maximum human pupil diameter under scotopic conditions, and a field of view of 120° , consistent with the functional limits of human vision, achieving the maximum angular resolving capacity of approximately 60 pixels per degree would require a display pixel density of around 23,000 pixels per inch (PPI). This value represents a conceptual benchmark rather than a practical specification, because under typical photopic conditions with a smaller pupil size (~ 4 mm) the required pixel density would be even higher. In practice, however, as the display is not intended to be positioned directly in the pupil plane (because of safety considerations and to satisfy optical invariants such as étendue), the resolution requirement can be relaxed, because increasing the eye–screen distance effectively enlarges the screen size.

Unfortunately, as pixel sizes continue to shrink in mainstream emissive displays, diminished emitter dimensions lead to reduced brightness, compromised uniformity, increased colour cross-talk and greater fabrication complexity, posing considerable challenges for ultra-high-resolution imaging^{1,2,3}. Currently, commercially available smartphone display pixels are typically around $60 \times 60 \mu\text{m}^2$ (~ 450 PPI), which is approximately 2,500 times larger than the theoretical size required for the ultimate retina display. Already at this scale, the emitted light becomes difficult for the naked eye to perceive, particularly in bright outdoor environments. Moreover, the smallest published colourful micro-light-emitting-diode (micro-LED) display currently available achieves only a pixel size of $4 \times 4 \mu\text{m}^2$ (excluding the distance between pixels)⁴,

making it challenging to replicate retinal-level resolution across vast fields of view. Furthermore, at such small scales, colour cross-talk and uniformity remain considerable technical hurdles. These limitations expose the large challenges of using conventional emissive display technology to realize the ultimate virtual reality display.

Reflective displays, which rely on ambient light for visibility, do not have luminosity issues, and their optical contrast remains unaffected by pixel size reduction given that reflection is governed by the polarization of materials at the nanoscale. However, existing reflective display (electronic paper or E-paper) technologies are hampered by marked limitations. Reflective liquid crystal displays, for instance, are constrained by the thickness of the liquid crystal layer, whereas electrophoretic displays (such as the Kindle) are restricted by the size of their capsules^{5,6}. So far no commercially available reflective display technology has achieved high resolutions of above 1,000 PPI.

Optical metasurfaces have demonstrated the capability to achieve ultra-high pixel densities of more than 10,000 PPI ($\sim 2.5 \mu\text{m}$ pixel size), with patterned nanomaterials capable of printing images at resolutions of up to around 100,000 dots per inch, approaching the optical diffraction limit^{7,8,9}. However, most modern nanoprinting methods rely on static materials, such as metals or high-refractive-index dielectrics^{10,11,12,13}. When applied to dynamic display systems (for example, meta-organic LED), these materials require modulation through micro-light sources, which are still affected by the inherent limitation of electromagnetic reduced intensity as resolution increases³. Furthermore, they are often affected by lateral light leakage between adjacent colour subpixels, limiting their ability to produce ultra-high-resolution images. In fact, static reflective displays are also influenced by interactions between neighbouring pixels, altering their optical properties at ultra-high pixel densities, making it challenging to use conventional red–green–blue (RGB) subpixel configurations for image display^{13,14,15}.

In recent years, there has been growing interest in integrating dynamic and static materials to explore tunable nanophotonics systems. Particularly in the field of displays, hybrid nanomaterials—combining tunable conjugated polymers or semiconductors as colour modulators with metallic

nanostructures—have demonstrated the ability to modulate the intensity or the reflected colours of subpixels^{16,17}. These technologies significantly enhance the colour gamut, reflectivity and optical contrast of E-paper and enable video display functionality^{18,19,20,21}. However, owing to limitations in structure, materials and fabrication methods, the pixel sizes of these hybrid nanomaterials remain in the range of tens to hundreds of micrometres, making it challenging to achieve ultra-high-resolution displays^{22,23,24}.

Here we propose a conceptually new E-paper technology, termed retina E-paper, capable of achieving ultra-high resolutions exceeding 25,000 PPI (~560 nm), surpassing the theoretical human visual limit of 60 pixels per degree across a 120° field of view on an 8 mm screen. The retina E-paper comprises electrochromic WO₃ metapixels, which undergo an insulator-to-metal transition during electrochemical insertion of, for example, alkali ions, allowing electrically dynamic control over optical properties such as refractive index and absorption. This transition enables tunable reflectance and contrast, which is critical for optimizing display performance. The basic colour generation principle builds on the hierarchical structuring of building blocks, Mie scattering and interference between the building blocks. This technology enables the practical construction of ultra-high-resolution displays (for example, exceeding 100 megapixels) within a compact area, paving the way for the ultimate virtual reality display.

The retina E-paper comprises electrochromic WO₃ metapixels integrated with a highly reflective substrate (Pt/Al). Its normalized high reflectance (~80%) and optical contrast (~50%) remain unaffected by pixel size reduction, maintaining exceptional visibility even at pixel sizes as small as approximately 400 nm. To minimize interference between adjacent pixels, we carefully optimized the dimensions and spacing of the primary colour metapixels, enabling full-colour displays by precisely mixing RGB subpixels. Furthermore, the substrate (Al/Pt) exhibits excellent conductivity. By reducing the lateral distance between the working and counter electrodes to 500 nm and using short-pulse input signals, we achieved greater than 95% optical contrast modulation of the WO₃ nanoparticles within 40 ms, supporting a video display of more than 25 Hz. This refresh rate is more than ten times faster than those of the previously reported fastest WO₃-based electrochromic devices²⁵. The short distance between the

working and counter electrodes enhances the external electric field driving ion doping, and this nanodisk design significantly reduces the required amount and increases the reaction surface area of WO_3 compared with the planar surface. Furthermore, unlike emissive displays that require constant power, retina E-paper features colour memory, consuming energy mainly during pixel switching. Its power usage is around 1.7 mW cm^{-2} for video and around 0.5 mW cm^{-2} for static images, significantly less than that of other types of E-reader²⁶.

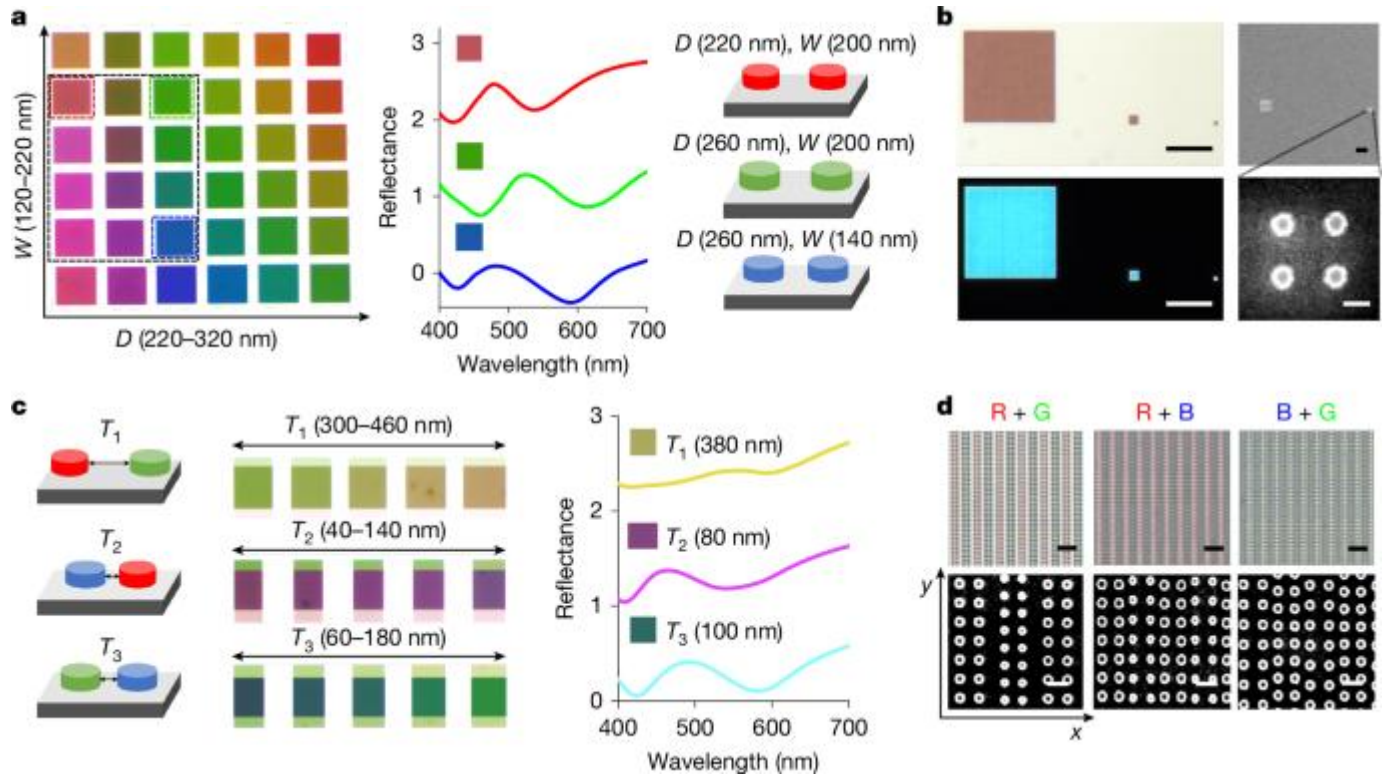
Finally, to demonstrate the potential of retina E-paper for virtual reality applications, we use cyan, magenta and yellow (CMY) colour metapixels to reconstruct an anaglyph 3D butterfly image. Furthermore, to showcase its full-colour display performance, we reproduced a high-resolution image inspired by the iconic painting *The Kiss* by Gustav Klimt and dynamically modulated the colours using electrical control. The retina E-paper features a compact surface area of around $1.9 \times 1.4 \text{ mm}^2$ (about 1/4,000th the size of a standard smartphone display) while achieving an impressive resolution of $4,300 \times 700$ pixels.

Figure 1b illustrates the fundamental structure of the retina E-paper, composed of electrochromic WO_3 metamaterials integrated with a highly reflective (Al/Pt) substrate. In the bright state, WO_3 behaves as a dielectric material with a high refractive index ranging from around 2 to 2.4 in the visible spectrum²⁷, enabling the generation of high-resolution colours even at sizes smaller than the incident wavelength¹¹. By precisely tuning the diameter (D) and spacing (W) of the nanodisks, the scattering modes can be adjusted to reflect the primary colours, RGB, forming the subpixels of one pixel of the retina E-paper. As the subpixels are made of meta-material, they are also called metapixels; however, optical interactions between these nanodisk-based subpixels can also affect colour mixing. Further tuning of the subpixel spacing (T) is required to ensure proper additive colour blending for display applications. After patterning the RGB subpixels, the next step is intensity modulation. As WO_3 is an electrochromic material, meta-atom absorption can be dynamically modulated by electrochemical reactions under applied voltage, altering the reflectivity of the subpixels. This capability enables the retina E-

paper to achieve dynamic colour modulation for display applications. The nanofabrication process is shown in Extended Data Fig. 1.

Figure 2a demonstrates how the reflective colours of WO_3 metapixels vary at a fixed thickness of 110 nm while varying the nanodisk diameter from 220 nm to 320 nm and the spacing from 100 nm to 200 nm. The thickness was chosen to balance Mie-resonance-based colour purity and electrochemical switching speed. Thinner layers may accelerate switching but reduce optical confinement and weaken Mie scattering, thus degrading colour saturation. This geometry range enables the metapixels to cover the entire visible spectrum. However, it is essential to note that not all RGB pixels are suitable for subpixels in retina E-paper. The reflected colour of each subpixel in an ultra-high-resolution E-paper system is influenced not only by its geometry but also by interactions with adjacent pixels (Fig. 2c). Therefore, selecting appropriate RGB pixels and ensuring that their hybrid reflected colours adhere to the principles of additive colour mixing is a critical step for achieving full-colour displays. In Fig. 2a (right), the spectra and corresponding geometries of the selected RGB pixels are presented: R ($D = 220$ nm, $W = 200$ nm), G ($D = 260$ nm, $W = 200$ nm) and B ($D = 260$ nm, $W = 140$ nm). The spectra are normalized to the reflective layer to highlight the WO_3 nanodisk colour-tuning by structural changes. Unlike emissive displays, in which visibility diminishes with pixel size reduction, E-paper technology maintains consistent brightness and reflectivity even at ultra-high resolutions. As illustrated in Fig. 2b, the red pixel retains its colour and reflectance in both bright- and dark-field microscope images, even as the size is reduced from 20 μm to 420 nm. A minimum of four nanodisks per pixel is required to preserve the Mie scattering and grating modes of the nanodisks, resulting in minimum pixel sizes of 420 nm for red, 460 nm for green and 400 nm for blue.

Fig. 2: Design and characterization of WO_3 metapixels.



a, Metapixel design. Left: tuning D and W of WO_3 nanodisks achieves a diverse colour palette. The dashed box highlights selected RGB pixels along with their intermediate regions, which contain CMY pixels. Middle: reflectance spectra of the selected RGB pixels. Right: corresponding D and W values for the chosen RGB pixels. **b**, Microscopic and structural characterization. Left: bright-field (top) and dark-field (bottom) microscope images of a red pixel with feature sizes of $20\ \mu\text{m}$, $2\ \mu\text{m}$ and $420\ \text{nm}$, captured under $\times 100$ magnification. Scale bars, $10\ \mu\text{m}$. Right: SEM images of $2\ \mu\text{m}$ and $420\ \text{nm}$ red pixels. Scale bars, $2\ \mu\text{m}$ (top) and $200\ \text{nm}$ (bottom). **c**, Colour mixing by subpixel arrangement. Left and middle: reflective colour varies as a function of T between adjacent RGB subpixels. Right: reflectance spectra of hybrid CMY pixels, corresponding to optimized subpixel spacing. **d**, High-resolution colour imaging. Top: bright-field microscope ($\times 100$) images of hybrid CMY pixels. Scale bars, $1\ \mu\text{m}$. Bottom: SEM images of the corresponding hybrid pixels. Scale bars, $500\ \text{nm}$.

Source Data

Once the smallest dimensions for the three primary colour metapixels are determined, the next step is merging them to achieve a full-colour display. In

Fig. 2c, the grating modes between adjacent subpixels are influenced by the spacing (T) between subpixels, which changes reflected hybrid colours. According to the principles of additive colour mixing, the overlap between RGB should produce CMY, respectively. As shown in Fig. 2a, the intermediate region (black dashed box) between RGB pixels also contains CMY pixels. As long as the spacing between RGB subpixels is carefully designed, the grating modes of adjacent pixels can produce CMY colours, ensuring compliance with the additive colour principle. For comparison, Extended Data Fig. 2 presents several arbitrarily selected combinations of RGB pixels that fail to reproduce the CMY colours. After carefully selecting RGB pixels and tuning the inter-pixel spacing—380 nm for red-green, 80 nm for blue-red and 100 nm for green-blue—the desired hybrid colours were successfully generated. The corresponding reflection spectra demonstrate that the reflectance of the hybrid-colour pixels matches that of the single-colour pixels.

Finally, Fig. 2d presents microscope and scanning electron microscope (SEM) images of the merged pixels producing CMY colours. Under high magnification ($\times 100$), the arrangement of alternating subpixels along the x axis to form hybrid colours is clearly visible. Notably, the Mie scattering mode of individual nanodisks is mainly determined by their size, whereas the grating mode of the subpixel arrays in the x direction governs the generation of reflective mixed colours.

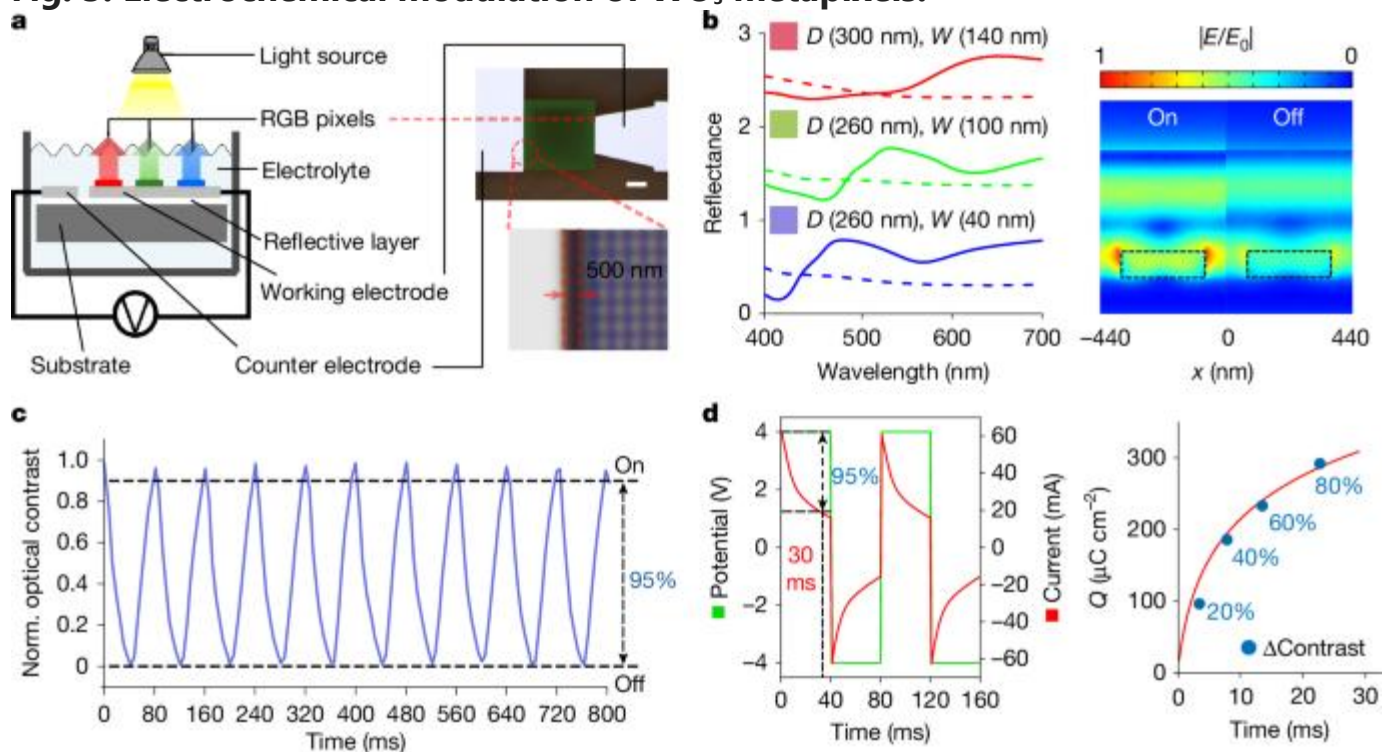
As an electrochromic material, WO_3 exhibits an electrically tunable refractive index (n) and extinction coefficient (k) across the visible spectrum (400–700 nm). In the insulator (colour) state, the refractive index varies from around 2.38 to 2.14, with k -values of < 0.01 . In the metal (black) state, n decreases from around 2.25 to 1.95, whereas k increases significantly ($k > 0.4$; Extended Data Fig. 3). This transition occurs on electrochemical reduction of WO_3 , when, for example, alkali ions or a proton, M^+ , are introduced into the material, altering its electronic structure. The reaction can be expressed as:

where M^+ represents the doping ion (for example, Li^+), x is the number of ions inserted into the WO_3 structure ($0 \leq x \leq 1$) and e^- represents an electron. When WO_3 is reduced, electrons are introduced into the conduction band comprising the W 5d bands. The injected electrons lead to the formation of localized

polarons, which result in a transition from insulating (semiconducting) behaviour to increased conductivity or metallic-like behaviour as x increases and the polarons overlap. As a result, the refractive index decreases and the extinction coefficient increases, contributing to the optical contrast between the insulating (clear) and metallic (dark) states. Furthermore, the nanodisk structure of the WO_3 metapixels, with its high refractive index (n), enables the concentration of incident light in the nanodisk. This effect further amplifies the light-matter interaction and absorption efficiency for stronger optical contrast.

Figure 3a presents the experimental set-up to electrochemically control the colour states of WO_3 metapixels. The electrolyte consists of 1 M LiClO_4 in acetonitrile, and the RGB pixel size is $350 \mu\text{m}$. Metallic electrodes (Pt/Al) were used to minimize potential drops. Notably, we designed a lateral electrode configuration with a narrow 500 nm gap between the working and counter electrodes, enhancing the local electric field and significantly improving the switching speed^{28,29}.

Fig. 3: Electrochemical modulation of WO_3 metapixels.



a, Experimental set-up for electrochemical characterization. Left: cross-sectional schematic diagram illustrating the set-up used to characterize the

optical properties of WO_3 metapixels under electrochemical control. Right: microscope images of the characterized sample show a 500 nm gap between the working and counter electrodes, which enhances the local electric field for improved switching performance. Scale bar, 100 μm . **b**, Optical response of electrochemically controlled RGB metapixels. Left: reflectance spectra of the selected RGB metapixels in their electrochemically modulated on (solid lines) and off (dashed lines) states, demonstrating dynamic tunability. Right: numerical simulation of the reflectance modulation of red metapixels at a 650 nm incident wavelength, validating that most of the electric field is concentrated in the WO_3 nanodisks. **c**, Switching speed characterization. By applying a short pulse voltage signal, 95% normalized optical contrast is achieved within 40 ms, demonstrating video-rate display applications. **d**, Electrical properties corresponding to optical modulation. Left: applied voltage pulses of ± 4 V with a 40 ms duration produce corresponding current responses, with 95% of the current change occurring within 30 ms, indicating fast ion transport in the WO_3 nanodisk structures. Right: relationship (turning off) between optical contrast change, response time and charge consumption. Owing to the colour memory effect of retina E-paper, video playback typically requires only minor updates, with intensity variations typically around 20% (equivalent to about 30 greyscale levels), thereby reducing the energy and time needed for dynamic content display.

Source Data

Figure 3b illustrates the measured normalized reflectance modulation of RGB metapixels in the on and off states. As both Mie scattering and grating modes are influenced by variations in the refractive index of the surrounding environment, the optimized nanodisk dimensions for the RGB metapixels are: R ($D = 300$ nm, $W = 140$ nm), G ($D = 260$ nm, $W = 100$ nm) and B ($D = 260$ nm, $W = 40$ nm). A clear distinction is observed when comparing the metapixel reflectance in air with that in electrolytes. Specifically, the reflectance in electrolytes is notably higher, whereas scattering in the red-light region is significantly suppressed. This effect arises because Mie scattering depends on the relative refractive index, where n_{particle} and n_{env} are the refractive index of the WO_3 nanodisks and the surrounding environment, respectively.

When n_{particle} is close to n_{env} , the scattering is markedly reduced, making the material seem more transparent and desaturated in colour. Therefore, the colour contrast of WO_3 metapixels in electrolytes is less saturated than in air; however, despite the ultra-thin WO_3 nanodisks (~ 100 nm), the optical contrast remains at $\sim 50\%$, significantly outperforming most planar WO_3 electrochromic devices with the same thickness³⁰. This enhancement is due to the high refractive index of WO_3 , concentrating the electric field of incident light in the nanodisks. After switching to the dark state, most of the incident light is absorbed, as confirmed by numerical simulations of red subpixel on and off states (Fig. 3b, right). The on–off switching of RGB pixels enables high-contrast modulation, which is essential for reflective display applications with full colour coverage.

Benefiting from the strong local electric field between the closely spaced working and counter electrodes, as well as the ultra-thin amorphous WO_3 nanodisks, yielding fast ion insertion³¹, the electrochemically tunable metapixels achieve an exceptionally fast switching time of only 40 ms to reach more than 95% of the total optical contrast modulation. Supplementary Video 1 demonstrates the rapid on–off switching of the red metapixel, confirming that metapixels support video display. Figure 3c shows ten cycles of reflectance variation in ± 4 V pulse input signals. The normalized optical contrast is calculated by $\frac{R - R_{\min}}{R_{\max} - R_{\min}}$, where R , R_{\min} and R_{\max} are the real-time, minimum and maximum reflectance of the WO_3 metapixels, respectively; this normalization clearly illustrates the change in optical contrast. The measured optical contrast is also shown in Extended Data Fig. 4. Notably, the operating voltage is comparable to the solid-state two-electrode WO_3 electrochromic systems³². However, due to the significantly enhanced switching speed (> 65 -times faster), precise pulsed voltage control—rather than a constant bias—can be used to minimize energy consumption and mitigate side effects.

Retina E-paper offers ultra-low energy consumption due to its inherent colour memory effect. Energy is primarily consumed when the pixel intensity is actively changed. As shown in Extended Data Fig. 5, pixels in the on state can retain more than 90% of their reflectance for more than 150 s without any power input. This indicates that for relatively static pixels, a brief, low-energy signal applied every several tens of seconds is sufficient to maintain the displayed content. Figure 3d presents the electrical characteristics associated with colour modulation in retina E-paper. Figure 3d (left) shows the current

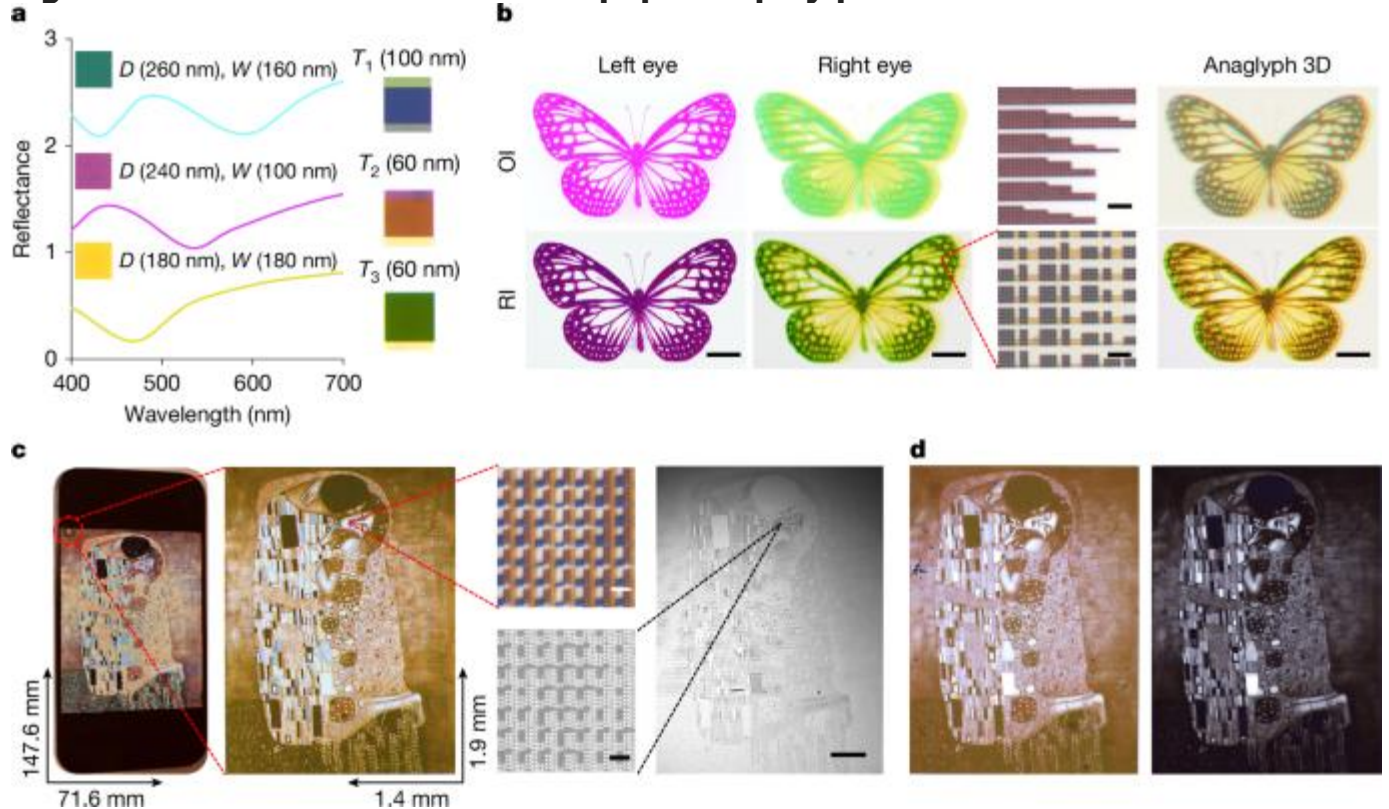
response to a ± 4 V voltage pulse, indicating that alkali ions can rapidly intercalate into the WO_3 nanodisk layer at video rates, thereby modulating pixel colour states. Figure 3d (right) illustrates the relationship between optical contrast change, response time and charge consumption. Importantly, during video playback, only about 10% of pixels typically undergo state changes²⁰, and among those, the average greyscale shift is around 30 levels³³. This means that, on average, only approximately 20% normalized optical contrast is required for video display. Under such conditions, retina E-paper achieves an average switching time of around 5 ms (200 fps) and an energy consumption of about 1.7 mW cm^{-2} . For static images, the energy use drops further to around 0.5 mW cm^{-2} . This energy consumption is significantly lower than that of conventional electrophoretic displays and electrowetting displays²⁶.

To further validate the display performance of retina E-paper, we fabricated metapixels to reproduce an anaglyph 3D butterfly and a high-resolution image inspired by *The Kiss*. The anaglyph butterfly demonstrates the feasibility of stereoscopic image rendering for virtual reality applications, whereas the reproduction of *The Kiss*—featuring intricate geometries and a wide colour gamut—highlights the suitability of retina E-paper for ultra-high-resolution, full-colour image display. As our substrate is a highly reflective material analogous to a white canvas, we used the CMY subpixels and used subtractive colour mixing to render the image. Importantly, the patterned image only demonstrates the display capability of WO_3 metapixels. For the display application, a thin-film transistor (TFT) array should be used to independently control the reflectance of each pixel, whereas the background should be set to black. The image rendering should follow the additive colour principle using RGB subpixels (Fig. 2).

Figure 4a (left) illustrates the nanodisk diameters and periodicities for the CMY metapixels alongside their corresponding reflection spectra, which show similar reflectance as RGB pixels. Figure 4a (right) presents the merged hybrid colour metapixels, in which the spacing between subpixels are B ($T_1 = 100 \text{ nm}$), R ($T_2 = 60 \text{ nm}$) and G ($T_3 = 60 \text{ nm}$). Notably, except for similar reflectance to RGB metapixels, the CMY system also ensures that the intermediate regions contain RGB pixels (Extended Data Fig. 6). The optimized nanodisk dimensions

for CMY pixels are C ($D = 260 \text{ nm}$, $W = 160 \text{ nm}$), M ($D = 240 \text{ nm}$, $W = 100 \text{ nm}$) and Y ($D = 180 \text{ nm}$, $W = 180 \text{ nm}$).

Fig. 4: Characterization of retina E-paper display performance.



a, Optical properties of CMY metapixels. Left: the reflectance spectra of the selected CMY metapixels demonstrate the spectral response. Right: photographs of the RGB pixels with optimized adjacent subpixel spacing for improved hybrid colour and display fidelity. **b**, Anaglyph 3D demonstration on retina E-paper. Left: the anaglyph stereo butterfly (Anaglyph 3D) original image (OI) decomposed into magenta (M) and cyan–yellow (CY) channels (top), and the corresponding reconstructed retina E-paper images (RI) for each eye (bottom). Scale bars, $200 \mu\text{m}$. Middle: microscope images of individual M and CY channel pixels, illustrating submicrometre pattern fidelity. Scale bars, $2 \mu\text{m}$. Right: full-colour anaglyph butterfly image: anaglyph 3D butterfly original image (top) and simulated retina E-paper reconstruction (bottom) demonstrating high-resolution 3D depth rendering. Scale bars, $200 \mu\text{m}$. Original butterfly image licensed from Adobe. **c**, High-resolution display of *The Kiss* on retina E-paper versus iPhone 15. Photographs comparing the display of *The Kiss* on an iPhone 15 and retina E-paper. The surface area of the

retina E-paper is $\sim 1/4,000$ times smaller than the iPhone 15. SEM and microscope images confirm that the displayed colours are generated by precisely arranged CMY subpixels. Scale bars, 2 μm (top and bottom left) 200 μm (right). Image of *The Kiss* reproduced with permission from Kingston Frameworks. **d**, Electrochemical display of *The Kiss* by retina E-paper. Photographs showing the display of *The Kiss* on retina E-paper in the on (left) and off (right) states, demonstrating reversible colour modulation when electrochemically tuned.

Source Data

Figure 4b illustrates an ultra-high-resolution anaglyph 3D display, achieved by encoding stereo image pairs (anaglyph 3D original image) into complementary colour channels—M for the left eye and CY for the right eye—and reconstructing them using the retina E-paper. This demonstration serves as a proof of concept for binocular disparity rendering, a fundamental mechanism underlying stereoscopic vision in virtual reality systems. As the retina E-paper does not connect to TFT arrays to individually adjust each subpixel, it achieves colour rendering solely through the precise geometric design of M–CY metapixels (Extended Data Fig. 7). By precisely reconstructing left and right eye images with submicrometre-resolution metapixels, the device successfully generates a full-colour 3D image (anaglyph 3D; Fig. 4b) through passive, compact optical configurations. This demonstrates an anaglyph 3D display with resolution exceeding 35,000 PPI (M) and 30,000 PPI (CY). Furthermore, this demonstration highlights the versatility of the retina E-paper platform, which can operate not only in full-colour mode but also in monochrome or dual-primary channel formats, broadening its applicability across a range of advanced display technologies.

Figure 4c presents a reconstructed full-colour image of *The Kiss*, directly comparing the retina E-paper with a commercial mobile-phone display (iPhone 15) in terms of both physical dimensions and display resolution. Whereas the iPhone screen measures 147.6 mm \times 71.6 mm, the retina E-paper is only 1.9 mm \times 1.4 mm, amounting to merely $\sim 1/4,000$ th the area of the smartphone display. Despite this minuscule size, the retina E-paper achieves a

resolution of $4,300 \times 700$, similar to the resolution of the smartphone display ($2,556 \times 1,179$). Due to the inherent challenges of accurately controlling the reflectance of subpixels, as well as the narrower colour gamut compared with emissive displays, the perceived colour saturation of the retina E-paper is lower than that of the iPhone 15; however, this is the first demonstration of full-colour imaging achieved by three primary colour metapixels at such an ultra-high resolution. With an average pixel size of only around 560 nm, the display reaches an unprecedented $>25,000$ PPI, surpassing the resolution requirements for ultimate virtual reality displays. High-magnification microscope ($\times 100$) and SEM images (Fig. 4b, right) further confirm the well-ordered CMY metapixel arrangement and the vibrant colour rendering, validating the ultra-high resolution of the retina E-paper.

To evaluate its electrically tunable colour performance, we reproduced *The Kiss* using CMY metapixels in an electrolyte environment. To maintain the presence of RGB pixels in the intermediate regions, the dimensions of the CMY metapixels were further optimized: C ($D = 280$ nm, $W = 20$ nm), M ($D = 220$ nm, $W = 80$ nm) and Y ($D = 300$ nm, $W = 80$ nm). The merged RGB subpixel spacing was adjusted accordingly: B ($T_1 = 40$ nm), R ($T_2 = 300$ nm) and G ($T_3 = 60$ nm) (Extended Data Fig. 8). Extended Data Fig. 9a presents the corresponding reflection spectra of CMY pixels in their colour and dark states. Figure 4d showcases the photos of *The Kiss* under colour and dark states in the electrolyte. Owing to the weaker Mie scattering of WO_3 nanodisks in an electrolyte environment compared with air, the displayed colours seem less saturated, with a noticeable reduction in extinction in the red region, resulting in an overall red-shifted colour. However, the system exhibits a distinct reflectance modulation between on and off states, highlighting its potential for dynamic display applications. Extended Data Fig. 9b compares the colour gamut coverage of commercial emissive displays, the retina E-paper in both air and electrolyte and the commercial colour electrophoretic display. Although the colour gamut of retina E-paper remains narrower than emissive displays, its performance in both air and electrolyte significantly surpasses a commercial colour E-reader³⁴.

Currently, more than 80% of the information people perceive is through visual signals³⁵. With the development of Internet-of-Things-based technology and

increasing information transfer speeds, the demand for next-generation visual display technologies keeps growing. Retina E-paper not only reaches the theoretical resolution limit of human vision but also offers exceptional visibility. It enables full-colour video display while maintaining high reflectivity and optical contrast, which is promising for realizing ultimate virtual reality displays.

Unlike conventional emissive displays, retina E-paper devices require front-illumination to enable image visibility. Extended Data Fig. 10 illustrates two distinct optical architectures that accommodate this requirement: one compatible with conventional virtual reality headsets, and the other tailored to state-of-the-art, waveguide-based augmented reality–virtual reality lenses³⁶. In fact, retina E-paper also holds significant potential for augmented reality applications, as it can leverage ambient light as the illumination source. This inherent compatibility with the environment enables natural visual integration, reducing reliance on light engines. Furthermore, as the primary illumination is provided by ambient light, its low power consumption enables substantial downsizing of the battery and even opens up the possibility of fully self-powered displays when combined with solar cells (with a typical output of $\sim 15 \text{ mW cm}^{-2}$).

Despite its advantages, retina E-paper requires further optimization in colour gamut, refresh rate, operational stability and lifetime. Lowering the operating voltage and exploring alternative electrolytes represent promising engineering routes to extend device durability and reduce energy consumption. Moreover, its ultra-high resolution also necessitates the development of ultra-high-resolution TFT arrays for independent pixel control, which will enable fully addressable, large-area displays and is therefore a critical direction for future research and technological development. Looking ahead, we anticipate significant advancements in this field and firmly believe that the evolution of the retina E-paper will ultimately influence everyone.

Methods

Nanofabrication of WO_3 nanodisks

We fabricated WO_3 nanodisk metamaterials (Extended Data Fig. 1) in a clean room using standard semiconductor processes. A 100 nm reflective layer (Al/Pt) and a 30 nm Au layer were deposited via electron beam evaporation (Lesker PVD 225). The middle 100 nm WO_3 layer was deposited using radio frequency magnetron sputtering. After spin-coating the electron beam resist (MaN 2401, 3,000 r.p.m.), nanostructures were patterned by electron beam lithography ($400 \mu\text{C cm}^{-2}$). The resist was developed in MF-24A for 45 s, followed by ion beam milling using Ar gas (80 mA, 200 V) for 2 min to etch the Au layer. Reactive ion etching with CF_4 gas (100 W) for 5 min was then used to etch the WO_3 layer. Finally, the Au layer was removed by wet etching. Samples were characterized using a Zeiss Supra 55 SEM for high-resolution imaging.

Electrochemical measurements

Acetonitrile was purchased from Sigma-Aldrich, and LiClO_4 was purchased from Fisher Scientific. The electrolyte contains 1 M LiClO_4 in acetonitrile. A custom-built liquid cell with two electrode connections was used for electrochemical measurements. A potentiostat (Gamry Interface 1000) controlled the applied current and voltage. For the fast-switching measurements, a short 40 ms voltage pulse ranging from -4 V to 4 V was applied. Low constant voltages from -1 V to 1 V were applied for 2 min to obtain the reference optical contrast of WO_3 .

Optical measurements

A custom microspectroscopy set-up with Thorlabs beam splitters was used to measure microscale reflectivity in the electrochemical cell. Illumination from a 100 W tungsten lamp and light collection was conducted through a $5\times$ air objective (NA 0.14), passing through the top flow cell with a glass cover into the WO_3 metapixels. A portion of the reflected light was collected by an optical fibre and analysed using a B&W Tek CypherX spectrometer. Most photographs were captured using a commercial microscope (Olympus MX50). An iPhone 15 and a Samsung A55 were used to capture the photograph in Fig. 4c (left) and Supplementary Video 1, respectively.

Arbitrarily selected combinations of RGB pixels

Extended Data Fig. 2 presents an example in which the intermediate regions of RGB pixels contain only cyan and yellow, but not magenta. Specifically, a yellow pixel ($D = 300$ nm, $W = 200$ nm) is observed, between the red ($D = 320$ nm, $W = 220$ nm) and green ($D = 260$ nm, $W = 200$ nm) pixels. Similarly, a cyan pixel ($D = 280$ nm, $W = 140$ nm) appears between the green and blue ($D = 280$ nm, $W = 120$ nm) pixels; however, the magenta pixel ($D = 260$ nm, $W = 100$ nm) is absent from the intermediate region between the red and blue pixels.

By adjusting subpixel spacing, a yellow pixel emerges when the red–green subpixel distance is 240 nm, whereas a cyan pixel forms at a blue–green subpixel distance of 120 nm; however, regardless of how the red–blue subpixel distance is tuned, magenta cannot be generated, contrasting with the results shown in Fig. 2c.

Refractive index of WO_3 in on–off states

The refractive index of WO_3 is obtained from a previously published study²⁵. Extended Data Fig. 3 presents both the real (n) and imaginary (k) components of the refractive index in both the on and off states. In the on state, the real part (n) decreases from 2.4 to 2.1, enabling strong Mie scattering in the air. The imaginary part (k), which represents optical absorption, remains close to zero, explaining why WO_3 nanodisks exhibit vivid colours in the air; however, in a liquid environment such as acetonitrile ($n \approx 1.33$), the refractive index is closer to that of WO_3 , reducing Mie scattering and making the nanodisks more transparent, thus diminishing colour vibrancy, as discussed in the main text. Electrochemical tuning in solution allows WO_3 nanodisks to switch to the off state, in which the k -value significantly increases to 0.05–0.4 in the visible range, leading to strong optical absorption and changing the colour pixels into dark states.

Optical contrast of red pixel

To compare with the normalized optical contrast shown in Fig. 3c, Extended Data Fig. 4 presents the absolute reflectance variation of red light at a wavelength of 620 nm in response to the applied 40 ms pulse voltage signal (Fig. 3d, left). The red subpixel achieves an optical contrast of more than 48%

within 40 ms, and its maximum optical contrast under long-time constant voltage is 50%. This result further confirms WO_3 metapixels supporting video display.

Colour memory effect

Owing to the bistability of WO_3 , the retina E-paper exhibits a colour memory effect. In the absence of external energy input, WO_3 gradually relaxes from its redox states back to the natural state, rather than reverting instantly from a coloured state to a dark state as seen in emissive displays. As shown in Extended Data Fig. 5, once a pixel is switched to the coloured mode, its normalized reflectance remains above 90% for around 150 s under open-circuit conditions. Similarly, when a pixel is switched to the dark mode, it retains a normalized reflectance less than 10% for about 9 s without further energy input. This behaviour enables ultra-low power consumption, as static or minimally changing pixels do not require continuous power. Instead, an approximately 2 ms electronic pulse input (for around 10% optical contrast modulation) is sufficient to maintain the display state.

CMY pixels in the air

As discussed in the main text, to achieve RGB colours through subtractive colour mixing using CMY primaries, it is crucial to ensure that the intermediate regions between CMY pixels contain RGB pixels. As shown in Extended Data Fig. 6, a blue pixel ($D = 260$ nm, $W = 120$ nm) exists between the cyan ($D = 260$ nm, $W = 160$ nm) and magenta ($D = 240$ nm, $W = 100$ nm) pixels. Similarly, a green pixel ($D = 260$ nm, $W = 180$ nm) is present between the magenta and yellow ($D = 180$ nm, $W = 180$ nm) pixels, while a red pixel ($D = 200$ nm, $W = 180$ nm) appears between the yellow and cyan pixels. By tuning the spacing between subpixels, a blue pixel emerges when the CM subpixel distance is 100 nm, green at an MY subpixel distance of 60 nm, and red at a CY subpixel distance of 60 nm.

Transfer colour image to nanodisk pixels

Extended Data Fig. 7 illustrates the process of converting the intensity (scaled from 0 to 255) of each CMY pixel into the geometry structure of nanodisk pixels. The intensity of each CMY channel is mapped to the height of its

corresponding CMY rectangle as a fraction of the maximum value, representing the percentage of light each CMY subpixel should reflect. The designated nanodisk arrays, which generate CMY colours, are then used to fill these rectangles, approximating the subpixel colour composition. However, due to the small size of the CMY rectangles, the nanodisks cannot achieve perfect spatial coverage, leading to inaccuracies in colour reproduction. This limitation contributes to the imperfections observed in Fig. 4b–d.

CMY pixels in the electrolyte

The underlying principle remains consistent with CMY pixels in the air. As illustrated in Extended Data Fig. 8, the intermediate regions of CMY colours contain corresponding RGB components. The subpixel distances are $T_1 = 40$ nm for blue, $T_2 = 300$ nm for red and $T_3 = 60$ nm for green. Owing to weaker Mie scattering in the electrolyte, the extinction of red colour becomes weaker, causing a less intense blue colour.

CMY colour modulation and comparison of colour performance with other devices

Extended Data Fig. 9a (left) illustrates the nanodisk diameters and periodicities for the CMY metapixels alongside their corresponding reflection spectra, which show similar reflectance as RGB pixels. The corresponding geometries are C ($D = 280$ nm, $W = 20$ nm), M ($D = 220$ nm, $W = 80$ nm) and Y ($D = 300$ nm, $W = 80$ nm), and the merged RGB subpixel spacing was adjusted accordingly: B ($T_1 = 40$ nm), R ($T_2 = 300$ nm) and G ($T_3 = 60$ nm).

Extended Data Fig. 9b presents a comparison of the colour gamut coverage among commercial emissive displays, the retina E-paper (under both air and electrolyte conditions), and a commercial colour electrophoretic display. Although the colour gamut of the retina E-paper does not yet match that of emissive technologies, it significantly outperforms existing commercial colour e-paper, highlighting its potential for high-fidelity reflective colour displays.

Front-illumination integration of retina E-paper into immersive augmented reality–virtual reality optics

Two potential system-level configurations are illustrated in Extended Data Fig. 10, demonstrating how reflective pixels can be effectively illuminated in practical augmented reality–virtual reality devices.

Extended Data Fig. 10a illustrates an optical configuration compatible with conventional virtual reality headsets. In this design, incident light enters from the side and is redirected by a beam splitter through an eyepiece onto the retina E-paper. The reflected light follows the reverse path, passing back through the eyepiece and beam splitter before reaching the eye. This optical arrangement resembles that of a reflective microscopy system and aligns with well-established principles in optical engineering.

Extended Data Fig. 10b depicts an advanced optical architecture compatible with waveguide-based augmented reality–virtual reality systems. In this configuration, light is side-coupled into the device and directed onto the retina E-paper through a beam splitter. The reflected light is then collimated and coupled into the waveguide through input gratings and ultimately delivered to the eye through output gratings. This design enables integration into compact form factors, significantly shortens the eye-to-display distance, and supports a wider field of view—key requirements for achieving immersive and lightweight augmented reality–virtual reality experiences.

Video-rate switching red pixel

Supplementary Video 1 visually demonstrates the rapid modulation speed of WO_3 metapixels by showing the reflectivity change of a red pixel under pulse signals with durations of 1 s, 500 ms, 250 ms and 40 ms. The distinct bright and dark states are clearly visible with evident dwell times, highlighting the full contrast range and switching stability of the device. Although the video was recorded by a cell phone at 50 fps, the camera of the microscope system was used to record the light spot at only 18 fps. As a result, despite the reaction speed exceeding the required for video play (24 fps), intensity variations remain observable.

.References

1. Joo, W. J. et al. Creating the ultimate virtual reality display. *Science* **377**, 1377–1378 (2022).
2. Lian, Y. et al. Downscaling micro- and nano-perovskite LEDs. *Nature* **640**, 62–68 (2025).
3. Joo, W. J. et al. Metasurface-driven OLED displays beyond 10,000 pixels per inch. *Science* **370**, 459–463 (2020).
4. Shin, J. et al. Vertical full-colour micro-LEDs via 2D materials-based layer transfer. *Nature* **614**, 81–87 (2023).
5. Kossyrev, P. A. et al. Electric field tuning of plasmonic response of nanodot array in liquid crystal matrix. *Nano Lett.* **5**, 1978–1981 (2005).
6. Zang, H. M. et al. Electrophoretic display comprising black, white, red, and yellow particles. *J. Soc. Inf. Disp.* **30**, 387–394 (2022).
7. Kumar, K. et al. Printing colour at the optical diffraction limit. *Nat. Nanotechnol.* **7**, 557–561 (2012).
8. Kuznetsov, A. I. et al. Optically resonant dielectric nanostructures. *Science* **354**, aag2472 (2016).
9. Proust, J. et al. All-dielectric colored metasurfaces with silicon Mie resonators. *ACS Nano* **10**, 7761–7767 (2016).
10. Bao, Y. et al. Full-colour nanoprint-hologram synchronous metasurface with arbitrary hue-saturation-brightness control. *Light Sci. Appl.* **8**, 95 (2019).
11. Yang, W. et al. All-dielectric metasurface for high-performance structural color. *Nat. Commun.* **11**, 1864 (2020).
12. Zheng, G. et al. Metasurface holograms reaching 80% efficiency. *Nat. Nanotechnol.* **10**, 308–312 (2015).
13. Cencillo-Abad, P. et al. Ultralight plasmonic structural color paint. *Sci. Adv.* **9**, adf7207 (2023).

- 14.Vynck, K. et al. The visual appearances of disordered optical metasurfaces. *Nat. Mater.* **21**, 1035–1041 (2022).
- 15.Song, M. et al. Versatile full-colour nanopainting enabled by a pixelated plasmonic metasurface. *Nat. Nanotechnol.* **18**, 71–78 (2023).
- 16.Kim, Y. et al. Active modulation of reflective structural colors. *Chem. Commun.* **58**, 12014–12034 (2022).
- 17.Peng, J. et al. Scalable electrochromic nanopixels using plasmonics. *Sci. Adv.* **5**, eaaw2205 (2019).
- 18.Duan, X. et al. Dynamic plasmonic colour display. *Nat. Commun.* **8**, 14606 (2017).
- 19.Xiong, K. et al. Plasmonic metasurfaces with conjugated polymers for flexible electronic paper in color. *Adv. Mater.* **28**, 9956–9960 (2016).
- 20.Xiong, K. et al. Video-rate switching of high-reflectivity hybrid cavities spanning all primary colors. *Adv. Mater.* **35**, 2302028 (2023).
- 21.Gugole, M. et al. Comparison of electrodeposited and sputtered tungsten trioxide films for inorganic electrochromic nanostructures. *ACS Appl. Opt. Mater.* **1**, 558–568 (2023).
- 22.Moon, C. et al. Active electrochemical high-contrast gratings as on/off switchable and color tunable pixels. *Nat. Commun.* **13**, 3391 (2022).
- 23.Xiong, K. et al. Switchable plasmonic metasurfaces with high chromaticity containing only abundant metals. *Nano Lett.* **17**, 7033–7039 (2017).
- 24.Xiong, K. et al. Active control of plasmonic colors: emerging display technologies. *Rep. Prog. Phys.* **82**, 024501 (2019).
- 25.Guo, J. et al. Fast-switching WO₃-based electrochromic devices: design, fabrication, and applications. *Acc. Mater. Res.* **4**, 438–447 (2023).
- 26.Fernández, M. R. et al. Review of display technologies focusing on power consumption. *Sustainability* **7**, 108543–110875 (2015).

27. Johansson, M. B. et al. Electronic and optical properties of nanocrystalline WO_3 thin films studied by optical spectroscopy and density functional calculations. *J. Phys. Condens. Matter* **25**, 205502 (2013).
 28. Xiong, K. et al. Video speed switching of plasmonic structural colors with high contrast and superior lifetime. *Adv. Mater.* **33**, 2103217 (2021).
 29. Greeuw, G. et al. Theoretical solution of the transient current equation for mobile ions in a dielectric film under the influence of a constant electric field. *J. Appl. Phys.* **9**, 3371–3375 (1984).
 30. Wen-Cheun Au, B. et al. Effect of film thickness on electrochromic performance of sol-gel deposited tungsten oxide (WO_3). *Opt. Mater.* **94**, 387–392 (2019).
 31. Bessinger, D. et al. Fast-switching vis-IR electrochromic covalent organic frameworks. *J. Am. Chem. Soc.* **143**, 7351–7357 (2021).
 32. Zhang, T. et al. Optical-cavity-incorporated colorful all-solid-state electrochromic devices for dual anti-counterfeiting. *Adv. Mater.* **36**, 2402670 (2024).
 33. Reddy, M. R. et al. Change detection in video using pixel based parametric analysis. *Indian J. Sci. Technol.* **8**, 35 (2015).
 34. Gugole, M. et al. Electrochromic inorganic nanostructures with high chromaticity and superior brightness. *Nano Lett.* **21**, 4343–4350 (2021).
 35. Qiu, T. et al. Vision-driven metasurfaces for perception enhancement. *Nat. Commun.* **15**, 1631 (2024).
 36. Yin, K. et al. Virtual reality and augmented reality displays: advances and future perspectives. *J. Phys. Photon.* **3**, 022010 (2021).
-